HHS Public Access

Author manuscript

ACS Nano. Author manuscript; available in PMC 2022 January 26.

Published in final edited form as:

ACS Nano. 2021 January 26; 15(1): 309–321. doi:10.1021/acsnano.0c03023.

Glycan-Modified Virus-Like Particles Evoke T Helper Type 1-Like Immune Responses

Mohammad Murshid Alam[†], **Cassie M. Jarvis**[#†,#], **Robert Hincapie**[#‡,#], **Craig S. McKay**[‡], **Jiri Schimer**[‡], **Carlos A Sanhueza-Chavez**[‡,¥], **Ke Xu**[§], **Roger C Diehl**[†], **M. G. Finn**[‡], **Laura L. Kiessling**[†,*]

[†]Department of Chemistry, Massachusetts Institute of Technology, Cambridge, MA, 02139 USA.

[‡]School of Chemistry and Biochemistry and School of Biological Sciences, Georgia Institute of Technology, 901 Atlantic Drive, Atlanta, GA, 30332, USA.

[¥]Current address: Department of Pharmaceutical Sciences, St. John's University, 8000 Utopia Pkwy. Queens, NY 11439, USA.

[§]Department of Biochemistry, University of Wisconsin-Madison, Madison, Wisconsin 53706, USA.

[#] These authors contributed equally to this work.

Abstract

Dendritic cells (DCs) are highly effective antigen-presenting cells that shape immune responses. Vaccines that deliver antigen to the DCs can harness their power. DC surface lectins recognize glycans not typically present on host tissue to facilitate antigen uptake and presentation. Vaccines that target these surface lectins should offer improved antigen delivery, but their efficacy will depend on how lectin targeting influences the T cell subtypes that result. We examined how antigen structure influences uptake and signaling from the C-type lectin DC-SIGN (dendritic cell-specific intercellular adhesion molecule-3-grabbing non-integrin, CD209). Virus-like nanoparticles (VLPs) were engineered from bacteriophage Qβ to present an array of mannoside ligands. The VLPs were taken up by DCs and efficiently trafficked to endosomes. The signaling that ensued depended on the ligand displayed on the VLP: only those particles densely functionalized with an aryl mannoside, Qβ-Man_{540}, elicited DC maturation and induced the expression of the proinflammatory cytokines characteristic of a T helper type 1 (T_H1)-like immune response. This effect was traced to differential binding to DC-SIGN at the acidic pH of the endosome. Mice were

[*]**Corresponding Author**: Laura L. Kiessling, kiesslin@mit.edu.
[#]These authors contributed equally.

Supporting Information

The Supporting Information is available free of charge.

Synthetic procedures and characterization data for new compounds including the arylmannoside and trimannose, VLP preparation and characterization data, ELISA data for binding of Qβ-Man_{540} and Qβ-$Man3_{200}$ to DC-SIGN at different pH, binding inhibition data for DC-SIGN and VLPs with ManLAM at different pH, images and early endosomal trafficking data of VLPs in Raji DC-SIGN cells, uptake of the Qβ-Man_{540} in the presence of anti-mannose receptor (CD206), anti-Dectin2 or anti-MINCLE antibody, gene silencing data using siRNA, volcano plot and heat maps of RNA-Seq data, anti-tumor immunity relevant cytokines and chemokine data derived from RNA-Seq analysis, model depicting the effect of pH on Qβ-Man_{540} and Qβ-$Man3_{200}$ binding and activation of DC-SIGN signaling pathway, list of top 100 upregulated genes in moDC stimulated with VLPs derived from RNA-Seq analysis, list of genes exclusively upregulated in moDC stimulated with VLP-Man_{540}, and a list of real time qPCR primer sequences.

The authors declare no competing financial interest.

immunized with a VLP bearing the aryl mannoside and a peptide antigen (Qβ-Ova-Man_{540}) had antigen-specific responses, including the production of $CD4^+$ T cells producing the activating cytokines interferon-γ and tumor necrosis factor-α. A T_H1 response is critical for intracellular pathogens (*e.g.*, viruses) and cancer; thus, our data highlight the value of targeting DC lectins for antigen delivery and validate the utility of DC-targeted VLPs as vaccine vehicles that induce cellular immunity.

Keywords

bacteriophage Qβ; dendritic cell; mannose; DC-SIGN; cytokines; T_H1 type immunity; virus-like particles

Dendritic cells (DCs) are the primary antigen-presenting cells that direct T cell differentiation. They help guide the immune response toward cellular or humoral immunity.[1] How to shift DC responses to elicit a specific outcome is unclear. Most subunit vaccines effectively induce T_H2 cells to afford robust antibody responses against extracellular pathogens. Cellular immunity to intracellular pathogens and cancer requires the induction of T_H1 cells. To generate T_H1-type immune responses, an ideal vaccine scaffold would readily be functionalized to incorporate antigens, deliver the antigens to the DCs, activated the desired intracellular signaling pathways, and provide self-adjuvating effects. We set out to test DC-targeting strategy using virus-like nanoparticles (VLPs).

Antigens can be targeted to DCs *via* endocytic receptors expressed on the cell surface. Many attractive targets are lectins, such as DC-specific intercellular adhesion molecule-3 grabbing non-integrin (DC-SIGN or CD209), dendritic cell-associated lectin-1 (dectin-1), dectin-2, mannose receptor, macrophage-inducible C-type lectin receptor (MINCLE), and DEC-205.[2, 3] These receptors could be used for antigen delivery, but many are expressed by other immune cells, limiting their utility to target DCs specifically. The C-type lectin receptor DC-SIGN, which is expressed predominantly on myeloid DCs,[4–6] is a tetrameric lectin that recognizes highly fucosylated and mannosylated antigens.[6] Soluble antigens that bind this receptor can undergo internalization and trafficking to endo-lysosomal compartments. These antigens are subsequently processed and presented on MHC class II molecules, which leads to $CD4^+$ T cell activation and differentiation. DC-SIGN can also route antigens for cross-presentation to elicit robust $CD8^+$ T cell responses.[3, 7–10] DC-SIGN can induce antigen-specific immune responses and present antigens to both $CD4^+$ and $CD8^+$ T cells, making it an attractive target for vaccine development.

Naturally occurring DC-SIGN ligands (*e.g.*, mannan, ManLAM, gp120, and Lewis antigens) can activate distinct intracellular signaling pathways that lead to either a T_H1 or T_H2 immune response,[4] underscoring the potential utility of DC-SIGN for immunomodulation.[11–13] A characteristic feature of effective DC-SIGN ligand interactions is multivalency. Thus, while conjugates of antigen or anti-DC-SIGN antibodies can engage DC-SIGN,[14–16] they do not mimic the extensive clustering that occurs upon binding highly multivalent glycans. The latter activate both DC-SIGN-mediated uptake and signaling.[17, 18] Antibody constructs lack toll-like receptor (TLR) ligands, and simultaneous engagement of DC-SIGN and TLRs amplifies signaling.[19] We tested the consequences of harnessing different factors

using a structurally well-controlled platform: synthetic glycans linked to a VLP. Using reliable methods of bioconjugation,[20] we anticipated that optimization of the identity, spatial distribution, and valency of the DC targeting agent would facilitate efficient antigen uptake and DC activation.[21] Because VLPs package nucleic acid TLR ligands, they can activate synergistic signals between the lectin and the TLRs.[19, 22]

The immunogenic properties of VLPs well known.[23–25] Here, we employ the highly stable particle derived from bacteriophage Qβ and use its many surface-exposed lysine residues[26–28] for ligand conjugation. These VLPs encapsidate bacterial RNAs, which can function as TLR agonists to provide self-adjuvanting effects. While VLPs have been reported to elicit $CD4^+$ T_H1 responses for high-affinity antibody production,[23, 29] they rarely promote the cellular T_H1 immune responses required for anti-cancer immunity.[30–31] We reasoned that targeting this platform to DC-SIGN might enhance antigen uptake[6] and activate lectin-augmented signaling[17, 18] to give rise to the desired T_H1 response.

As described below, we found that both the density and the nature of the DC-SIGN binding ligand matter. Specifically, VLPs densely substituted with an aryl mannoside elicited proinflammatory, T_H1-type signaling pathways and cytokine expression, leading to induction of T_H1 cells *in vivo*. T_H1-type cells that support cellular immunity are critical for effective responses against tumors and intracellular pathogens such as certain bacteria and viruses.[16, 32, 33] Thus, our findings highlight the promise of DC-targeted VLP constructs and identify critical features needed for the T cell immunity that underlies therapeutic and prophylactic vaccines.

Results and Discussion

DC-SIGN recognizes and internalizes antigens bearing mannosylated glycans.[17, 34] We displayed both components on the icosahedral Qβ VLP (hydrodynamic diameter ~36 nm, Figure S2). This particle comprises 180 copies of a 14 kDa coat protein, each with its N-terminus and three lysine residues exposed on the outer surface, accounting for up to 720 amine conjugation sites.[27, 28] We expected that higher densities of ligand presentation would increase binding avidity to the tetrameric DC-SIGN receptor and promote the receptor clustering needed for antigen uptake and intracellular signaling.

VLPs were treated with a low concentration of a succinimidyl ester-bearing fluorophore (Alexa Fluor 488) to attach approximately 20 dyes per particle, and then with a high concentration of an azide-terminated succinimidyl ester linker. Virtually all of the accessible amino groups were thereby acylated, resulting in a random and even distribution of azides on the particle surface. These intermediate particles were then decorated with one of two forms of alkyne-functionalized mannose ligands. Because of the presence of a hydrophobic pocket near the carbohydrate-binding site,[35, 36] we used an α-O-aryl mannoside derivative (Man, Figure 1).[34] We also examined a trimannoside (Man3, Figure 1), which lacks the aryl substituent. We reasoned these tailored particles would provide the means to compare how different DC-SIGN ligands impact VLP uptake and DC signaling. As a non-binding group, we used the pentaerythritol-derived triol (PE) to mimic the polyhydroxylated nature of the carbohydrate but not its receptor-relevant structure.

The density of Man and Man3 functionalization on the particle was controlled by mixing each of these alkynes with the PE-alkyne in varying ratios. Each mixture was used in a copper(I)-catalyzed azide-alkyne cycloaddition (CuAAC) reaction in the presence of tris(3 hydroxypropyltriazolylmethyl)amine (THPTA),[26] providing complete conversion of VLP-azides to triazoles. Mass spectrometry analysis established that the ratios of mannosyl and PE units attached to the particle closely matched their feed ratio, as expected from the assumption that all of the alkynes were equally reactive.[37] To achieve its highest loading of the trimannoside, the Man3 alkyne was used alone with no admixed PE-alkyne. In each case, some lysines on the inside surface of the capsid shell were also modified (as inferred from the overall quantitation derived from mass spectrometry). The number of ligands designated for each construct is the approximate number of *exterior-surface* attachments made, based on our estimation that approximately 30% of modifications under high-loading conditions are made to interior-surface lysine residues.

Particles bearing the following average numbers of ligands were generated: Qβ-Man_{540}, Qβ-Man_{90}, Qβ-$Man3_{475}$, and Qβ-$Man3_{200}$ (Figure 1). As mentioned above, VLPs bearing only the PE group (Qβ-PE_{540}) served as controls, as they do not bind DC-SIGN. The resulting VLP conjugates were characterized by analytical size-exclusion chromatography and dynamic light scattering (DLS) and found to be >95% intact. Assuming that the ionization efficiencies of all of the protein subunits are similar, the extent of labeling could be estimated by ESI-MS (Figure S1–3, Table S1). In this way, stable VLPs with well-controlled variations in the identity (aryl mannoside, pentaerythritol, trimannoside) and the density of the functionalizing unit allowed us to examine how VLP structure influences DC responses.

DC-SIGN-mediated particle uptake

To assess VLP uptake *via* DC-SIGN, we compared VLP binding and internalization into two matched cell lines-- Raji cells and a Raji cell line engineered to produce DC-SIGN (Raji/DC-SIGN) (Figure 2).[34] While flow cytometry reports does not directly report on internalization, our previous results indicated that the signals track with DC-SIGN-mediated uptake of mannosylated particles.[34] The densely mannosylated particles, Qβ-Man_{540}, Qβ-$Man3_{475}$, and Qβ-$Man3_{200}$, were taken up by selectively only by the cell line expressing DC-SIGN (Figure 2a). In contrast, the non-mannosylated Qβ-PE_{540} and the sparsely mannosylated Qβ-Man_{90} were barely recognized. Little signal was detected with Raji cells lacking DC-SIGN (Figure 2b). Mannose-rich VLPs were also avidly bound and internalized by human monocyte-derived dendritic cells (moDCs) (Figure 2c). In the experiment, the sparsely mannosylated and control PE-decorated particles gave low but detectable signals, consistent with observations that a wide variety of protein nanoparticles can undergo receptor-mediated endocytosis and other processes such as macropinocytosis.[38–40]

We tested whether uptake of the mannosylated VLPs depended on DC-SIGN. The addition of the calcium chelator EDTA significantly diminished VLP uptake, consistent with the role of calcium in carbohydrate-recognition by DC-SIGN[41] (Figure 2d). Also, an anti-DC-SIGN antibody (anti-CD209, Figure 2e) inhibited VLP uptake, but antibodies against the mannose receptor (CD206), dectin-2, or Mincle had little or no effect (Figure S10). These data

support the conclusion that efficient internalization of Qβ-Man_{540}, Qβ-$Man3_{475}$ and Qβ-$Man3_{200}$ VLPs requires DC-SIGN.

Highly mannosylated VLPs traffic efficiently to endosomal compartments

Immature DCs take up, process, and present antigen to specific T-cell clones to induce immune responses.[42–44] The loading of antigen into MHCs for T cell presentation depends on particle trafficking to endosomal compartments for proteolytic processing.[45] We anticipated that the VLPs would be efficiently directed to endosomal compartments, giving rise to both DC-SIGN and TLR signaling along with engagement of endosomal TLR7 by VLP-packaged ssRNA to promote immune activation. The intracellular trafficking of highly mannosylated particles in the moDCs was investigated by fluorescence microscopy, using standard markers of early and late endosomes (transferrin and LAMP2, respectively). We observed particle colocalization with each marker for all of the Qβ VLPs (Figure 3, S9). These observations indicate that though the mannose density strongly influences the extent of VLP uptake, all of the nanoparticles, once internalized, traffic similarly and efficiently to the endosomal compartments that lead to antigen processing.

Induction of DC maturation and expression of proinflammatory and TH1-type cytokines

After antigen encounter, immature DCs undergo maturation, a process characterized by high expression of MHC II and costimulatory molecules.[46] We observed that moDCs treated with Qβ Man_{540}, Qβ-$Man3_{475}$, or Qβ-$Man3_{200}$ showed increases in MHC II, but only Qβ-Man_{540} led to higher CD86 levels (Figure 4b). CD86 relays signals necessary for T cell activation and survival; therefore, we postulated that only Qβ-Man_{540} would selectively augment signaling between TLRs and DC-SIGN to induce cytokines that promote DC maturation[47, 48] and specific immune responses.[4, 22] We therefore examined the cytokine profiles elicited by various glycandecorated VLPs.

Quantitative PCR measurements in moDCs after stimulation with VLPs confirmed that Qβ-Man_{540} elicited a unique profile of cytokine expression. Specifically, this VLP promoted robust expression of proinflammatory and T_H1-type cytokines (IL-1β, IL-6, IL-8, IL-12B, interferon-β (IFNβ), and tumor necrosis factor (TNF)), but not the T_H1 inhibitory cytokine IL-10 (Figure 5a–g).[49–51] IL-12 was the most dramatically upregulated, and this cytokine induces production of the transcription factor T-bet (TBX21) that directs T_H1 cell differentiation.[52] Only Qβ-Man_{540} elicited the production of the bioactive form of IL-12p70, which promotes T_H1 cell differentiation[19, 22] (Figure 5h). Treatment of moDCs with anti-DC-SIGN antibody before Qβ-Man_{540} addition led to reduced cytokine expression (Figure 6a–e). Thus, the ability of Qβ-Man_{540} to elicit T_H1 responses depends on DC-SIGN engagement.

DC-SIGN clustering promotes dendritic cell activation. The DC-SIGN signaling complex consists of scaffolding proteins LSP1 (lymphocyte-specific protein 1), KSR1 (kinase suppressor of Ras 1), CNKSR1 (connector enhancer of KSR1), and the protein kinase Raf-1. When multivalent mannose derivattives engage DC-SIGN signaling occurs to induce the recruitment of effector proteins that activate Raf-1.[4, 22] This signaling cascade results in the phosphorylation and acetylation of the NF-κB subunit p65 and the production of IL-12p70.

Thus, loss of LSP or Raf-1 activity should hamper Qβ-Man_{540} signaling. Indeed, knockdown of LSP1 and Raf-1 in moDCs using small interfering RNA (siRNA, Figure S11) decreased the Qβ-Man_{540}-induced expression of IL-6, IL-12B, and IFNβ (Figure 6f–h). This finding supports our hypothesis that Qβ-Man_{540} - induced cytokine expression results from an intact DC-SIGN signaling complex.

Differential binding of Qβ-Man_{540} and Qβ-$Man3_{200}$ to DC-SIGN at acidic pH values

VLPs bearing either the trimannose or the aryl mannoside were recognized by DC-SIGN and underwent similar levels of DC internalization (Figure 2a, c). However, only the aryl mannoside-bearing particles induced significant cytokine expression. This difference did not depend on the average loading of mannose-based epitopes (Qβ-Man_{540} *versus* Qβ-$Man3_{475}$) or the total mannose residues displayed (Qβ-Man_{540} *versus* Qβ-$Man3_{200}$). Antigen internalization and signaling rely on DC-SIGN engagement on the cell surface and in the endosome, and the pH of each environment differs. We therefore assessed DC-SIGN binding to Qβ-Man_{540} and Qβ-$Man3_{200}$ as a function of pH. We found Qβ-Man_{540} and Qβ-$Man3_{200}$ to bind with roughly equal avidities to the DC-SIGN extracellular domain (ECD) at pH 7.4. At lower pH, however, Qβ-$Man3_{200}$ lost roughly half of its binding power whereas Qβ-Man_{540} binding was unchanged (Figure 7, S9b–d). Similar differences were also observed in a competitive binding assay using mannose-capped lipoarabinomannan (ManLAM) (Figure S10). The affinity of DC-SIGN for carbohydrates diminishes drastically at pH 5.5 and below because coordination to calcium ions decreases at low pH values.[53, 54]

The results above indicate that only Qβ-Man_{540} interacts with DC-SIGN in the acidic endosomal compartments. Such stability would enhance DC-SIGN mediated signaling and its synergism with that of endosomal-resident Toll-like receptors such as TLR7. The latter can be activated by the release of ssRNA as the VLP capsid is degraded. We attribute the pH insensitivity of the DC-SIGN– Qβ-Man_{540} aryl mannoside complex to the dense display of ligands with an aryl group, which can engage in hydrophobic and CH-π interactions[55] that are not as pH-dependent as calcium-binding. Given Qβ-Man_{540}'s ability to be taken up, initiate signal transduction, and activate immunostimulatory TH1 cell-polarizing cytokine expression, we tested whether it could shape adaptive immunity.

Transcriptional analysis of moDCs treated with mannosylated particles

We probed the consequences of VLP exposure on moDCs using a global transcriptome analysis. RNA sequencing revealed significant upregulation of 927 genes in moDCs treated with Qβ-Man_{540} (false discovery rate (FDR)-adjusted $P < 0.05$). The aryl mannoside-modified particles (Qβ-Man_{540}) elicited more changes in gene expression than did Qβ-$Man3_{200}$ or control Qβ-PE_{540} (246 and 436 upregulated genes, respectively). No significant differences were observed between Qβ-$Man3_{200}$ and control Qβ-PE_{540} (Figure S12, 11, Table S2). Analysis of expressed cytokine/immunity-related genes showed 281 genes were upregulated upon Qβ-Man_{540} treatment, indicating the aryl mannoside-conjugated particle is a more potent inducer of cytokine responses (Figure 8a, Table S3). Pathway analysis showed that the Qβ particles, regardless of their modification, can induce multiple genes with interconnected functions in innate and adaptive immunity. Overall, the particles activate intracellular signaling, including pathways related to innate immune (pattern recognition

receptor or PRR) activation, dendritic cell maturation, NF-kB activation, as expected based on their immunostimulatory TLR agonists.[56] In contrast to this generic effect, Qβ-Man_{540} activated a significantly higher number of genes related to cellular immunity (Figure 8c). Specifically, Qβ-Man_{540} stimulation promoted significant activation of the T_H1 signaling pathway. The activation z-score for the T_H1 pathway (z-score: 2.5) is significant compared to the z-score of the T_H2 pathway (z-score: 0.6), underscoring the ability of the Qβ-Man_{540} to skew T_H1 signaling in DCs.

Induction of T_H1-type immune responses *in vivo*

Differentiation of naïve T cells into appropriate T_H cell subtypes is critical for mounting efficient T cell responses and shaping immunity. T_H1 cell responses are required for host defense against intracellular pathogens including viruses and certain bacteria or tumors, and T_H2 cell responses are critical for immunity to extracellular pathogens.[57–59] Dendritic cells orchestrate the differentiation process by stimulating T cell receptors *via* antigen presentation and by triggering a specialized cytokine microenvironment. To test whether DC-SIGN-targeted particles stimulate effective *in vivo* antigen responses, we created hybrid particles that displayed both the Ova323–329 peptide (a model antigen) and an aryl mannoside. Thus, the VLPs were generated such that approximately 32 of the 180 subunits displayed the peptide at the C-terminus.[60] Each Ova323 sequence was preceded on the peptide extension by a linker sequence that could be cleaved by the endosomal protease cathepsin D Ova323 peptide to promote efficient antigen processing and presentation.[61] These particles were then decorated with the aryl mannoside or trimannoside recognition elements as before to afford structures designated Qβ-Man_{540}-Ova, Qβ-$Man3_{200}$-Ova and Qβ-PE_{540}-Ova (Figure 9a, S4–6). Since the Ova323 peptide contains no lysine residues, it could not undergo chemical modification; therefore, the bioconjugation steps were assumed to give rise to very similar arrays of DC-SIGN ligand as before.

Six-week-old C57BL/6J mice were immunized three times (at 2-week intervals) with Qβ-Man_{540}-Ova, Qβ-$Man3_{200}$-Ova or Qβ-PE_{540}-Ova (Figure 9b).[62] Blood was drawn for detection of Ova-specific IgG antibody on days 14, 28, and 35 to monitor the development of antibody responses following each dose relative to pre-immune levels (day 0). On day 35 (7 days following the last dose), the mice were sacrificed, and their spleens were isolated for immune cell analysis. We pulsed splenocytes with Ova peptide and used intracellular cytokine staining to quantify the percentage of $CD4^+$ T cells expressing IFN-γ and TNF-α. Compared with the unvaccinated control, we observed a significant increase ($P<0.05$) in the percentage of IFN-γ and TNF-α producing $CD4^+$ T cells in Qβ-Man_{540}-Ova immunized mice (Figure 9c, d). Notably, a higher percentage of $CD4^+$ T cells secreted the cytokines characteristic of T_H1-type polyfunctional T cells (Figure 9e). Thus, Qβ-Man_{540}-Ova activated mouse DCs and, by virtue of Ova peptide presentation, induced the differentiation of naïve helper T cells into T_H1 cells *in vivo*. ELISPOT analysis also showed a strong induction of IFN-γ production upon *ex vivo* stimulation of isolated splenocytes with Ova peptide (Figure 9f). We did not observe any IFN-γ response when these splenocytes were stimulated with bovine serum albumin (BSA) (data not shown). This enhancement was observed only for mice immunized with particles bearing both the peptide and the aryl

mannoside ligand. These data are consistent with our *in vitro* results as only the VLPs that potently activate immune signaling give rise to the expected T cell responses.

Serum ELISA analyses showed that Qβ-Man_{540}-Ova immunized mice produced lower anti-Ova IgG antibody responses than mice immunized with Qβ-$Man3_{200}$-Ova or Qβ-PE_{540}-Ova (Figure 9g). This decrease in antibody production is consistent with the expectation that the aryl mannoside-decorated VLP biases differentiation away from T_H2 cells and concomitant antibody production. Indeed, DC secretion of cytokines such as IFN-γ and IL-12 promotes T_H1 and inhibits T_H2 differentiation (Figure 5e, 5f, 5h).[63–65] This finding is unexpected: the inclusion of a robust DC-SIGN ligand shifts the immune response away from antibody production and toward cellular immunity.

Conclusion

Using a small-molecule, DC-SIGN ligand, we have generated a Qβ protein nanoparticle that gives rise to a tailored immune response. Robust engagement of DC-SIGN, even at lower pH, shifted the immune response away from antibody production and toward cellular immunity. Several molecular factors contributed to this outcome, including the use of an aryl O-glycoside, its dense display on the protein nanoparticle, and the introduction of a peptide antigen that does not interfere with DC-SIGN binding or antigenic processing. The induction of T_H1 cells in coordination with cytotoxic T cells has great potential for controlling tumors and developing protective immunity against viruses. Loss of T_H1 cells during viral infection[66] can be overcome by therapeutically reconstructing T_H1 responses and therefore restoring anti-viral $CD8^+$ T cell immunity. Thus, T_H1 response can offset immunosuppression and offer an effective vaccination strategy. Combining the immunogenic properties of VLP scaffolds with DC-SIGN engagement may offer an augmented platform for both prophylactic and therapeutic vaccination.

Methods and materials

Cells and animals.

Adult human peripheral blood was acquired from Research Blood Components, LLC (Boston, MA) or drawn under University of Wisconsin-Madison IRB approved protocol from healthy volunteers. Monocytes were isolated from whole blood by negative selection using RosetteSep human monocyte enrichment cocktail following manufacturers protocol (StemCell Technologies). Using density gradient medium (Lymphoprep) monocytes were isolated and differentiated into immature DCs in the presence of GM-CSF (100 ng/mL) and IL-4 (50 ng/mL) (R&D Systems) in CellGenix GMP DC media (CellGenix) for 6 to 7 days. For cytokine analysis and RNA-Seq moDCs were treated with 4 nM VLPs for 6 h at 37 °C in a humid atmosphere with 5% CO_2. Raji and Raji DC-SIGN cells were cultured and maintained as described previously.[17] Briefly, cells were maintained in RPMI (Gibco) supplemented with 10% fetal bovine serum and penicillin/streptomycin at 37 °C in a humid atmosphere with 5% CO_2.

C57BL/6 mice were purchased from Jackson Laboratory and were used at 6–8 weeks of age. All experiments were approved by the Institutional Animal Care and Use Committee (IACUC) of University of Wisconsin-Madison.

Expression and purification of Qβ VLPs.

Wild-type Qβ particles and hybrid Qβ-Ova particles were expressed and isolated as previously described.[60, 67] Briefly, chemically competent BL21(DE3) cells were transformed with pET28CP or simultaneously transformed with pET28CP/pCDFCP-Ova, plated onto SOB-agar containing appropriate antibiotics, and grown overnight. After 24 h, a single well-isolated colony was inoculated into 25 mL SOB media containing antibiotics. Following overnight growth, cultures were diluted into 500 mL selective SOB media and incubated at 37 °C. Cultures were grown to OD_{600} between 0.7–0.9, and protein expression was induced by the addition of isopropyl β-D-1-thiogalactopyranoside (IPTG) to a final concentration of 1 mM. Following incubation for 5 h at 37 °C, cells were harvested by centrifugation (6,000 rpm, 10 min) and frozen at −80 °C until processing for particle isolation.

Frozen cell pellets were resuspended in 0.1 M potassium phosphate buffer, pH 7.4 and lysed by probe sonication (10 min on total, 75 W, 5 sec on, 5 sec off) in an ice bath. Lysates were clarified by centrifugation (14,000 rpm, 10 min) and VLPs were precipitated from the cell lysate supernatant by addition of 27% $(NH_4)_2SO_4$ (w/v) and subsequent gentle shaking at 4 °C for a minimum of 1 h. The protein precipitate was collected by centrifugation (14,000 rpm, 10 min) and resuspended in 0.1 M potassium phosphate buffer. To remove lipids and aggregates, an organic extraction was performed by addition of 1 volume of an n-BuOH/$CHCl_3$ solution [1:1 (v/v)]. The VLP-containing aqueous layer was removed following centrifugation (14,000 rpm, 10 min) and particles were further purified by 10–40% sucrose gradient ultracentrifugation (25,000 rpm, 4 h). Visible particle-containing bands were extracted, and particles isolated by ultracentrifugation (68,000 rpm, 2 h). VLP pellets were decanted, resuspended in 0.1 M potassium phosphate buffer, and sterilized by 0.2 μm PTFE syringe filters.

Characterization of Qβ VLPs.

Protein concentration was determined by a Bradford assay (Pierce, Coomassie Plus) against BSA standards. Particles were characterized by FPLC using a Superose 6 size exclusion column to determine particle purity and aggregation and by dynamic light scattering using a Wyatt Dynapro plate reader to determine hydrodynamic radius. Particle encapsulation of endogenous RNA from *E. coli* was determined by UV absorption of native protein samples measured at 260 nm and 280 nm. Qβ VLPs contain few aromatic amino acids that contribute to UV absorbance measurements. Hydrolysis of encapsulated nucleic acids in Qβ was performed using a standard procedure[68] to provide a background measurement for the absorbance. Incorporation of the C-terminal extended cathepsin D sensitive tag-Ova monomers into hybrid particles was assessed by ESI-TOF HRMS and by microfluidic electrophoretic analysis using a Bioanalyzer protein chip and was determined to be approximately 32 copies per particle. The full sequence of the extension monomer is (Qβ −8AA linker-*cathepsin D sensitive tag*-**OvaII**):

AKLETVTLGNIGKDGKQTLVLNPRGVNPTNGVASLSQAGAVPALEKRVTVSVSQPSR
N
RKNYKVQVKIQNPTACTANGSCDPSVTRQAYADVTFSFTQYSTDEERAFVRTELAAL
LA SPLLIDAIDQLNPAY-GGASESGA-*DGSPLEF*-**ISQAVHAAHAEINEAGR**.

Note: molar concentration values given for VLPs in various experiments refer to the concentration of particles, each composed of 180 capsid subunits and containing encapsulated ssRNA.

Fluorescent labeling and mannosylation of Qβ VLPs.

Both WT and hybrid particles were fluorescently labeled and mannosylated by a similar two-step protocol. Amine-reactive succinimidyl ester chemistry was used to install the fluorophore and an azide, followed by mannoside-alkyne ligation *via* the copper-catalyzed azide-alkyne cycloaddition. Alexa Fluor 488 NHS ester (0.1 μmol) was added to a solution of Qβ VLPs (2 mg, 0.14 μmol CP subunit) and after 4 h of gentle mixing at 4 °C, NHS-azide (4.0 μmol) was added. The reaction was allowed to proceed overnight. The reaction mixture was purified using a PD-10 desalting column, followed by concentrating using centrifugal filtration using an Amicon Ultra 100k MW cut-off device. The extent of particle modification was determined *via* ESI-MS and electrophoretic analysis. The resulting azide-modified particles were treated with ligand-alkyne in the presence of coppersulfate, Tris((1-benzyl-4-triazolyl)methyl)amine or THPTA, aminoguanidine, and sodium ascorbate. Mannoside loading was controlled by addition of different concentrations of the arylmannoside alkyne or trimannose-alkyne, as described in the supporting information. A control pentaerythritol monoether ligand was used to cap the remaining azides. Upon completion, reactions were purified by PD-10 desalting columns, followed by centrifugal filtration using an Amicon Ultra 100k MW cut-off device. Protein recovery was determined *via* a Bradford assay and particles were characterized as described above to determine particle stability, purity, and the extent of modification.

Assessing Qβ VLP internalization.

The moDCs, Raji or Raji-DC-SIGN cells were suspended in PBS (pH 7.4) supplemented with 1 mM $CaCl_2$ and 0.5 mM $MgCl_2$ at 0.5×10^6 cells/mL. Cells were stimulated with 2 nM of the functionalized Qβ-AF488 at 37 °C for the indicated time points. To inhibit the uptake of VLPs, moDCs were pretreated with anti-human CD209 (5 μg/ml) antibody for 20 min on ice and incubated with the VLPs at 37 °C as described above for 15 min. Similarly, the uptake of the VLPs were inhibited by EDTA (1 mM). The extent of VLP internalization was measured by flow cytometry. Data were analyzed using FlowJo software (V.10.4) utilizing the mean fluorescence intensity (MFI) to quantify VLP internalization. Where indicated, the data was normalized to the MFI of the unstimulated cells.

DC activation and maturation.

MoDC activation and maturation was determined by measuring the expression of CD86 and HLA-DR (MHC II). In a 24-well tissue culture plate 0.25×10^6 moDC were treated with 4 nM VLPs for 24 h at 37 °C in a humid atmosphere with 5% CO_2. Subsequently cells were stained with anti-human CD86-APC or HLA-DR-PE-Cy5 antibody (BD Bioscience) for 30

min on ice. The presence of the relevant proteins was evaluated by flow cytometry. Data were analyzed by FlowJo software (V.10.4) to calculate mean fluorescence intensity (MFI) as a measure of expression.

Cell stimulation and quantitative real-time PCR.

Cytokine expression was measured by quantitative real-time PCR (qPCR) following 6 h incubation of the moDC with 4 nM functionalized Qβ VLPs. To investigate whether the cytokine expression depended on DC-SIGN, cells were preincubated for 2 h with 20 μg/ml anti-CD209 antibody prior to stimulation with the VLPs. Total RNA was extracted with Trizol using Direct-zol™ RNA Kits (Zymo Research). cDNA was generated by using iScript cDNA Synthesis Kit (BioRad) and PCR amplification was performed in the presence of SYBR green (BioRad) in a CFX96 Real-Time PCR Detection System (BioRad) or an ABI 7500 Fast PCR detection system (Applied Biosystems). Specific primers were designed using the PrimerQuest tool (Integrated DNA Technologies, Inc., Supplementary Table 3). Expression of specific genes was normalized to GAPDH expression (ΔCt) and expression fold change was calculated using the delta Ct method ($2^{-(\Delta Ct\ Stim-\ \Delta Ct\ Unstim)}$).

IL-12p70 ELISA.

The moDCs were stimulated with 4 nM functionalized Qβ VLPs for 48 h at 37 °C with 5% CO_2, and the supernatants were collected for analysis using a human IL-12p70 Quantikine ELISA kit (R&D Systems, Minneapolis, MN) according to the manufacturer's protocol.

DC-SIGN ECD and VLP binding ELISA.

To assess binding of DC-SIGN to mannose functionalized VLPs, ELISA plates were coated with Qβ-Man_{540} or Qβ-$Man3_{200}$ (2 μg/mL) in PBS at 4^{o} C for overnight. The plates were incubated with two fold serially diluted DC-SIGN ECD[69] (3.2 μg/ml to 0.003 μg/ml in HEPES buffer containing 20 mM HEPES, 150 mM NaCl, 10 mM $CaCl_2$, 0.1% BSA and 0.1% Tween) at pH 7.4, 6.0, 5.5 and 5.0 for 1 h at RT. The presence of bound DC-SIGN ECD was detected using horseradish peroxidase-conjugated anti-DC-SIGN (B2) IgG antibody (Santa Cruz Biotechnology). After 1 h incubation at RT, the plates were developed with tetramethlybenzidine (TMB) for 20 min. The optical density (OD) was measured at 450 nm after addition of 0.5 M sulfuric acid to the plates using microplate reader (Bio-tek Elx 800). The apparent K_d was calculated by nonlinear regression curve fit for total binding using GraphPad Prism.

RNA interference of DCs.

The moDCs were transfected with 25 nM SMARTpool small interfering RNAs (siRNAs) including LSP1, Raf-1, GPAD, and nontargeting siRNA as a control using transfection reagents DF4 according to the manufacturer's protocol (Dharmacon). After 26 h of transfection, cells were stimulated with 4 nM Qβ-$(Man)_{540}$ for 6 h and RNAs were extracted for gene expression analysis. Gene silencing and cytokine expression was verified by qPCR.

RNA-Sequencing.

Total RNA was extracted using Trizol and Direct-zol™ RNA Kits as described above. RNA sequencing and differential gene expression analysis was performed by University of Wisconsin-Madison Biotechnology Center. Ingenuity Pathway Analysis (IPA; QIAGEN) was used to identify top pathways being upregulated and to identify putative upstream regulators responsible for differential gene expression signatures. Gene enrichment score analysis was performed using a method described previously.[70] Briefly, to calculate the gene enrichment score, gene signatures were obtained from the literature for anti-viral,[71, 72] inflammatory,[71] anti-cancer (melanoma),[73] and tolerogenic genes.[74] The expression values for the specific genes were normalized by dividing by the average expression of the gene in unstimulated cells and the geometric means for the specific list of genes were calculated to obtain the “Gene Enrichment Score”.

Microscopy.

To measure early endosomal trafficking of the particles, moDCs (0.5×10^6 cells/mL) were incubated with Cy3-transferrin (8 μg/mL, Jackson Immunoresearch) for 30 min in 1% BSA/RPMI. Cells were washed and treated with 2 nM VLPs for the indicated time periods at 37 ^{o}C and then placed on ice prior to washing and transferring cells to LabTek II Chambered Coverglass (#1.5). To measure late endosomal trafficking of the particles, cells were treated with 2 nM VLPs as above, fixed in 2% formaldehyde, washed, permeabilized in 0.05% saponin/PBS and stained using rat anti-Lamp2 antibody (Santa Cruz Biotechnology) and donkey anti-rat IgG-Alexa Fluor 594 (Invitrogen). Cells were imaged on a Nikon A1R confocal microscope, 60X objective, 60 μm pinhole. Co-localization analysis was performed in Fiji using the colocalization threshold plugin to obtain the Pearson’s Coefficient.

Mouse immunization and sampling.

C57BL/6 mice were randomly divided into different cohorts and immunized subcutaneously with 50 μg of Qβ-Man_{540}-Ova, Qβ-$Man3_{200}$-Ova or Qβ-PE_{540}-Ova. Mice were immunized on days 0, 14, and 28, using Complete Freund’s Adjuvant (CFA) for the first immunization and Incomplete Freund’s Adjuvant (IFA) for the subsequent boosts. Blood samples were collected *via* tail bleeds on days 0, 14, 28 and 35. Serum samples were collected, processed, aliquoted, and stored as described previously.[75] For intracellular cytokine staining and ELISPOT assay, splenocytes were isolated at day 35 and processed for flow cytometry as described below.

Intracellular Cytokine Staining.

Splenocytes were isolated from mice following a protocol described elsewhere.[75] Splenocytes were resuspended at a concentration of 2×10^6 cells/ml in RPMI medium supplemented with 10% FBS and cultured in U-bottom tissue culture plates (Nunc, Denmark) in the presence of $Ova_{323–339}$ peptide (5 μg/ml) or phorbol myristate acetate (PMA)-ionomycin cocktail (Invitrogen) as a positive control. Samples containing unstimulated cells were included as a negative control. Splenocytes and antigens were incubated for 1 h at 37 °C in 5% CO_2. After 1 h, brefeldin A (BFA; BD Biosciences) was added and cell cultures were incubated for an additional 5 h. Following the 6 h stimulation,

cells were washed with phosphate-buffered saline (PBS) and stained with Ghost Dye Red 780 (Tonbo Biosciences), cell surface monoclonal antibodies: anti-CD3-PE (Clone 17A2) and anti-CD4-APC (Clone RM4–5) (BD Biosciences). Following surface staining, cells were permeabilized using BD cytofix/cytoperm plus fixation/permeabilization kit following manufacturers protocol (BD Bioscience, San Jose). Permeabilized cells were washed and then stained for 30 min at 4 °C with fluorochrome-conjugated antibodies (*i.e.*, anti-IFN-γ-PE-Cy7 and anti-TNF-α-PerCP-Cy5.5; BD Biosciences). Following staining, cells were washed, and flow cytometry was performed using a FACS LSRII. Net stimulation was calculated by subtracting the frequency of parent (FOP) of the unstimulated cells from the FOP of the antigen-stimulated cells.

IFNγ enzyme-linked immune absorbent spot (ELISPOT).

Splenocytes were isolated from naïve and Qβ-Man_{540}-Ova immunized mice as described above. In each well 5×10^5 cells were stimulated for 18 h with 5 μg/mL Ova323 in RPMI 1640 supplemented with 10% FBS at 37 °C under 5% CO_2. IFN-γ- secreting cells was measured using mouse IFN-γ ELISPOT kit following the manufacturer instructions (R&D Systems).

Detection of antibody response in serum.

Anti-Ova IgG antibody response was measured in serum using standard enzyme-linked immunosorbent assay (ELISA) protocols.[75] Briefly, ELISA plates were coated with Ova peptide (1μg/mL) in PBS at 4 °C overnight. To each well, 100 μL of serum (diluted 1:250 in 0.1% BSA in phosphate buffered saline-Tween 20) was added and the presence of Ova-specific antibodies was detected using horseradish peroxidase-conjugated anti-mouse IgG (diluted 1:500 in 0.1% BSA in phosphate buffered saline-Tween 20) (Jackson ImmunoResearch). After 1.5 h incubation at room temperature (RT), the plates were developed with tetramethlybenzidine (TMB), and the optical density at 630 nm was determined using an Infinite M1000 microplate reader (Tecan Trading AG, Switzerland). Plates were read for 6 min at 60 s intervals, and the data was reported as millioptical density units per minute (mOD/min). The data was normalized to ELISA units by calculating the ratio of the optical density of the test sample to that of a standard of pooled sera from mice vaccinated with ovalbumin from a previous study (manuscript in preparation) on the same plate.

Statistical analysis.

Statistical analyses were performed using GraphPad Prism 7 (GraphPad Software, Inc., La Jolla, CA). Wilcoxon matched-paired signed rank test, one-way or two-way ANOVA with multiple comparisons tests were performed as indicated. All reported *P* values were two tailed and statistical significance was defined as a *P* value of <0.05.

Supplementary Material

Refer to Web version on PubMed Central for supplementary material.

Acknowledgements.

This research was supported by the National Institutes of Health (AI055258). The authors acknowledge the University of Wisconsin-Madison Biotechnology Center Gene Expression Center & DNA Sequencing Facility for library preparation and next generation sequencing. Additionally, the authors thank J. Hank, P. Sondel, J. Olsen and M. Cook of University of Wisconsin-Madison and N. Mehta and K. Wittrup of Massachusetts Institute of Technology for their technical support and advice with the mouse experiments.

References

1. Moser M; Murphy KM, Dendritic Cell Regulation of Th1-Th2 Development. Nat Immunol 2000, 1, 199–205. [PubMed: 10973276]
2. Johannssen T; Lepenies B, Glycan-Based Cell Targeting to Modulate Immune Responses. Trends Biotechnol 2017, 35, 334–346. [PubMed: 28277249]
3. Garcia-Vallejo JJ; Ambrosini M; Overbeek A; van Riel WE; Bloem K; Unger WW; Chiodo F; Bolscher JG; Nazmi K; Kalay H; van Kooyk Y, Multivalent Glycopeptide Dendrimers for the Targeted Delivery of Antigens to Dendritic Cells. Mol Immunol 2013, 53, 387–397. [PubMed: 23103377]
4. Geijtenbeek TB; Gringhuis SI, C-Type Lectin Receptors in the Control of T Helper Cell Differentiation. Nat Rev Immunol 2016, 16, 433–448. [PubMed: 27291962]
5. Geijtenbeek TB; Torensma R; van Vliet SJ; van Duijnhoven GC; Adema GJ; van Kooyk Y; Figdor CG, Identification of DC-SIGN, a Novel Dendritic Cell-Specific ICAM-3 Receptor That Supports Primary Immune Responses. Cell 2000, 100, 575–585. [PubMed: 10721994]
6. van Kooyk Y; Unger WW; Fehres CM; Kalay H; Garcia-Vallejo JJ, Glycan-Based DC-SIGN Targeting Vaccines to Enhance Antigen Cross-Presentation. Mol Immunol 2013, 55, 143–145. [PubMed: 23158834]
7. Singh SK; Stephani J; Schaefer M; Kalay H; Garcia-Vallejo JJ; den Haan J; Saeland E; Sparwasser T; van Kooyk Y, Targeting Glycan Modified Ova to Murine DC-SIGN Transgenic Dendritic Cells Enhances MHC Class I and II Presentation. Mol Immunol 2009, 47, 164–174. [PubMed: 19818504]
8. Unger WW; van Beelen AJ; Bruijns SC; Joshi M; Fehres CM; van Bloois L; Verstege MI; Ambrosini M; Kalay H; Nazmi K; Bolscher JG; Hooijberg E; de Gruijl TD; Storm G; van Kooyk Y, Glycan-Modified Liposomes Boost CD4+ and CD8+ T-Cell Responses by Targeting DC-SIGN on Dendritic Cells. J Control Release 2012, 160, 88–95. [PubMed: 22366522]
9. Tacken PJ; Ginter W; Berod L; Cruz LJ; Joosten B; Sparwasser T; Figdor CG; Cambi A, Targeting DC-SIGN *Via* Its Neck Region Leads to Prolonged Antigen Residence in Early Endosomes, Delayed Lysosomal Degradation, and Cross-Presentation. Blood 2011, 118, 4111–4119. [PubMed: 21860028]
10. Tacken PJ; de Vries IJM; Torensma R; Figdor CG, Dendritic-Cell Immunotherapy: From *Ex Vivo* Loading to *In Vivo* Targeting. Nat. Rev. Immunol. 2007, 7, 790–802. [PubMed: 17853902]
11. Hodges A; Sharrocks K; Edelmann M; Baban D; Moris A; Schwartz O; Drakesmith H; Davies K; Kessler B; McMichael A; Simmons A, Activation of the Lectin DC-SIGN Induces an Immature Dendritic Cell Phenotype Triggering Rho-GTPase Activity Required for HIV-1 Replication. Nat Immunol 2007, 8, 569–577. [PubMed: 17496896]
12. Chiodo F; Marradi M; Park J; Ram AF; Penades S; van Die I; Tefsen B, Galactofuranose-Coated Gold Nanoparticles Elicit a Pro-Inflammatory Response in Human Monocyte-Derived Dendritic Cells and Are Recognized by DC-SIGN. ACS Chem Biol 2014, 9, 383–389. [PubMed: 24304188]
13. Gringhuis SI; Kaptein TM; Wevers BA; Mesman AW; Geijtenbeek TB, FucoseSpecific DC-SIGN Signalling Directs T Helper Cell Type-2 Responses Via IKKepsilon- and CYLD-Dependent BCL3 Activation. Nat Commun 2014, 5, 3898. [PubMed: 24867235]
14. Unger WW; Mayer CT; Engels S; Hesse C; Perdicchio M; Puttur F; Streng-Ouwehand I; Litjens M; Kalay H; Berod L; Sparwasser T; van Kooyk Y, Antigen Targeting to Dendritic Cells Combined with Transient Regulatory T Cell Inhibition Results in Long-Term Tumor Regression. Oncoimmunology 2015, 4, e970462.
15. Hesse C; Ginter W; Forg T; Mayer CT; Baru AM; Arnold-Schrauf C; Unger WW; Kalay H; van Kooyk Y; Berod L; Sparwasser T, In Vivo Targeting of Human DC-SIGN Drastically Enhances

CD8(+) T-Cell-Mediated Protective Immunity. Eur J Immunol 2013, 43, 2543–2553. [PubMed: 23784881]

16. Velasquez LN; Stuve P; Gentilini MV; Swallow M; Bartel J; Lycke NY; Barkan D; Martina M; Lujan HD; Kalay H; van Kooyk Y; Sparwasser TD; Berod L, Targeting Mycobacterium tuberculosis Antigens to Dendritic Cells Via the DC-Specific-ICAM3-Grabbing-Nonintegrin Receptor Induces Strong T-Helper 1 Immune Responses. Front Immunol 2018, 9, 471. [PubMed: 29662482]
17. Prost LR; Grim JC; Tonelli M; Kiessling LL, Noncarbohydrate Glycomimetics and Glycoprotein Surrogates as DC-SIGN Antagonists and Agonists. ACS Chem Biol 2012, 7, 1603–1608. [PubMed: 22747463]
18. Kiessling LL; Grim JC, Glycopolymer Probes of Signal Transduction. Chem Soc Rev 2013, 42, 4476–4491. [PubMed: 23595539]
19. Gringhuis SI; den Dunnen J; Litjens M; van Het Hof B; van Kooyk Y; Geijtenbeek TB, C-Type Lectin DC-SIGN Modulates Toll-Like Receptor Signaling *Via* Raf-1 Kinase-Dependent Acetylation of Transcription Factor NF-KappaB. Immunity 2007, 26, 605–616. [PubMed: 17462920]
20. Strable E; Finn MG, Chemical Modification of Viruses and Virus-Like Particles. In: Manchester M, Steinmetz NF (eds) Viruses and Nanotechnology. Current Topics in Microbiology and Immunology, 2009, vol 327, pp 1–21. Springer, Berlin, Heidelberg.
21. Fasting C; Schalley CA; Weber M; Seitz O; Hecht S; Koksch B; Dernedde J; Graf C; Knapp EW; Haag R, Multivalency as a Chemical Organization and Action Principle. Angew Chem Int Ed Engl 2012, 51, 10472–10498. [PubMed: 22952048]
22. Gringhuis SI; den Dunnen J; Litjens M; van der Vlist M; Geijtenbeek TB, Carbohydrate-Specific Signaling through the DC-SIGN Signalosome Tailors Immunity to *Mycobacterium tuberculosis*, HIV-1 and *Helicobacter pylori*. Nat Immunol 2009, 10, 1081–1088. [PubMed: 19718030]
23. Braun M; Jandus C; Maurer P; Hammann-Haenni A; Schwarz K; Bachmann MF; Speiser DE; Romero P, Virus-Like Particles Induce Robust Human T-Helper Cell Responses. Eur J Immunol 2012, 42, 330–340. [PubMed: 22057679]
24. Frietze KM; Peabody DS; Chackerian B, Engineering Virus-Like Particles as Vaccine Platforms. Curr Opin Virol 2016, 18, 44–49. [PubMed: 27039982]
25. Polonskaya Z; Deng S; Sarkar A; Kain L; Comellas-Aragones M; McKay CS; Kaczanowska K; Holt M; McBride R; Palomo V; Self KM; Taylor S; Irimia A; Mehta SR; Dan JM; Brigger M; Crotty S; Schoenberger SP; Paulson JC; Wilson IA et al., T Cells Control the Generation of Nanomolar-Affinity Anti-Glycan Antibodies. J Clin Invest 2017, 127, 1491–1504. [PubMed: 28287405]
26. Hong V; Presolski SI; Ma C; Finn MG, Analysis and Optimization of Copper-Catalyzed Azide-Alkyne Cycloaddition for Bioconjugation. Angew Chem Int Ed Engl 2009, 48, 9879–9883. [PubMed: 19943299]
27. Golmohammadi R; Fridborg K; Bundule M; Valegard K; Liljas L, The Crystal Structure of Bacteriophage Q Beta at 3.5 Å Resolution. Structure 1996, 4, 543–554. [PubMed: 8736553]
28. Rumnieks J; Tars K, Crystal Structure of the Bacteriophage Qbeta Coat Protein in Complex with the Rna Operator of the Replicase Gene. J Mol Biol 2014, 426, 1039–1049. [PubMed: 24035813]
29. Skibinski DA; Hanson BJ; Lin Y; von Messling V; Jegerlehner A; Tee JB; Chye de H; Wong SK; Ng AA; Lee HY; Au B; Lee BT; Santoso L; Poidinger M; Fairhurst AM; Matter A; Bachmann MF; Saudan P; Connolly JE, Enhanced Neutralizing Antibody Titers and Th1 Polarization from a Novel *Escherichia coli* Derived Pandemic Influenza Vaccine. PLoS One 2013, 8, e76571. [PubMed: 24204639]
30. Storni T; Ruedl C; Schwarz K; Schwendener RA; Renner WA; Bachmann MF, Nonmethylated CG Motifs Packaged into Virus-Like Particles Induce Protective Cytotoxic T Cell Responses in the Absence of Systemic Side Effects. J Immunol 2004, 172, 1777–1785. [PubMed: 14734761]
31. Molino NM; Anderson AK; Nelson EL; Wang SW, Biomimetic Protein Nanoparticles Facilitate Enhanced Dendritic Cell Activation and Cross-Presentation. ACS Nano 2013, 7, 9743–9752. [PubMed: 24090491]

32. Borkow G; Bentwich Z, Host Background Immunity and Human Immunodeficiency Virus Protective Vaccines, a Major Consideration for Vaccine Efficacy in Africa and in Developing Countries. Clin Diagn Lab Immunol 2002, 9, 505–507. [PubMed: 11986252]
33. Haabeth OA; Lorvik KB; Hammarstrom C; Donaldson IM; Haraldsen G; Bogen B; Corthay A, Inflammation Driven by Tumour-Specific Th1 Cells Protects against B-Cell Cancer. Nat Commun 2011, 2, 240. [PubMed: 21407206]
34. Jarvis CM; Zwick DB; Grim JC; Alam MM; Prost LR; Gardiner JC; Park S; Zimdars LL; Sherer NM; Kiessling LL, Antigen Structure Affects Cellular Routing through DC-SIGN. Proc Natl Acad Sci U S A 2019, 116, 14862–14867. [PubMed: 31270240]
35. Schuster MC; Mann DA; Buchholz TJ; Johnson KM; Thomas WD; Kiessling LL, Parallel Synthesis of Glycomimetic Libraries: Targeting a C-Type Lectin. Org Lett 2003, 5, 1407–1410. [PubMed: 12713285]
36. Van Liempt E; Imberty A; Bank CM; Van Vliet SJ; Van Kooyk Y; Geijtenbeek TB; Van Die I, Molecular Basis of the Differences in Binding Properties of the Highly Related C-Type Lectins DC-SIGN and L-SIGN to Lewis X Trisaccharide and *Schistosoma Mansoni* Egg Antigens. J Biol Chem 2004, 279, 33161–33167. [PubMed: 15184372]
37. Kislukhin AA; Hong VP; Breitenkamp KE; Finn MG, Relative Performance of Alkynes in Copper-Catalyzed Azide-Alkyne Cycloaddition. Bioconjug Chem 2013, 24, 684–689. [PubMed: 23566039]
38. Sabharwal P; Amritha CK; Sushmitha C; Natraj U; Savithri HS, Intracellular Trafficking and Endocytic Uptake Pathway of Pepper Vein Banding Virus-Like Particles in Epithelial Cells. Nanomedicine (Lond) 2019, 14, 1247–1265. [PubMed: 31084385]
39. Al-Barwani F; Young SL; Baird MA; Larsen DS; Ward VK, Mannosylation of Virus-Like Particles Enhances Internalization by Antigen Presenting Cells. PLoS One 2014, 9, e104523.
40. Win SJ; Ward VK; Dunbar PR; Young SL; Baird MA, Cross-Presentation of Epitopes on Virus-Like Particles *Via* the MHC I Receptor Recycling Pathway. Immunol Cell Biol 2011, 89, 681–688. [PubMed: 21221122]
41. Feinberg H; Mitchell DA; Drickamer K; Weis WI, Structural Basis for Selective Recognition of Oligosaccharides by DC-SIGN and DC-SIGNR. Science 2001, 294, 2163–2166. [PubMed: 11739956]
42. Zinkernagel RM; Doherty PC, Restriction of *In Vitro* T Cell-Mediated Cytotoxicity in Lymphocytic Choriomeningitis within a Syngeneic or Semiallogeneic System. Nature 1974, 248, 701–702. [PubMed: 4133807]
43. Doherty PC; Zinkernagel RM, H-2 Compatibility Is Required for T-Cell-Mediated Lysis of Target Cells Infected with Lymphocytic Choriomeningitis Virus. J Exp Med 1975, 141, 502–507. [PubMed: 123002]
44. Zinkernagel RM; Callahan GN; Althage A; Cooper S; Klein PA; Klein J, On the Thymus in the Differentiation of “H-2 Self-Recognition” by T Cells: Evidence for Dual Recognition? J Exp Med 1978, 147, 882–896. [PubMed: 305459]
45. Compeer EB; Flinsenberg TW; van der Grein SG; Boes M, Antigen Processing and Remodeling of the Endosomal Pathway: Requirements for Antigen Cross-Presentation. Front Immunol 2012, 3, 37. [PubMed: 22566920]
46. Manicassamy S; Pulendran B, Dendritic Cell Control of Tolerogenic Responses. Immunol Rev 2011, 241, 206–227. [PubMed: 21488899]
47. Radvanyi LG; Banerjee A; Weir M; Messner H, Low Levels of Interferon-Alpha Induce CD86 (B7.2) Expression and Accelerates Dendritic Cell Maturation from Human Peripheral Blood Mononuclear Cells. Scand J Immunol 1999, 50, 499–509. [PubMed: 10564553]
48. Zou GM; Tam YK, Cytokines in the Generation and Maturation of Dendritic Cells: Recent Advances. Eur Cytokine Netw 2002, 13, 186–199. [PubMed: 12101074]
49. Hanada T; Tanaka K; Matsumura Y; Yamauchi M; Nishinakamura H; Aburatani H; Mashima R; Kubo M; Kobayashi T; Yoshimura A Induction of Hyper Th1 Cell-Type Immune Responses by Dendritic Cells Lacking the Suppressor of Cytokine Signaling-1 Gene. J Immunol 2005, 174, 4325–4332. [PubMed: 15778397]

50. Trinchieri G, Interleukin-12 and the Regulation of Innate Resistance and Adaptive Immunity. Nat Rev Immunol 2003, 3, 133–146. [PubMed: 12563297]
51. Kadowaki N; Antonenko S; Lau JY; Liu YJ, Natural Interferon Alpha/Beta-Producing Cells Link Innate and Adaptive Immunity. J Exp Med 2000, 192, 219–226. [PubMed: 10899908]
52. O'Shea JJ; Lahesmaa R; Vahedi G; Laurence A; Kanno Y, Genomic Views of STAT Function in CD4+ T Helper Cell Differentiation. Nat Rev Immunol 2011, 11, 239–250. [PubMed: 21436836]
53. Tabarani G; Thepaut M; Stroebel D; Ebel C; Vives C; Vachette P; Durand D; Fieschi F, DC-SIGN Neck Domain Is a pH-Sensor Controlling Oligomerization: SAXS and Hydrodynamic Studies of Extracellular Domain. J Biol Chem 2009, 284, 21229–21240. [PubMed: 19502234]
54. Snyder GA; Ford J; Torabi-Parizi P; Arthos JA; Schuck P; Colonna M; Sun PD, Characterization of DC-SIGN/R Interaction with Human Immunodeficiency Virus Type 1 Gp120 and ICAM Molecules Favors the Receptor's Role as an Antigen-Capturing Rather Than an Adhesion Receptor. J Virol 2005, 79, 4589–4598. [PubMed: 15795245]
55. Hudson KL; Bartlett GJ; Diehl RC; Agirre J; Gallagher T; Kiessling LL; Woolfson DN, Carbohydrate-Aromatic Interactions in Proteins. J Am Chem Soc 2015, 137, 15152–15160. [PubMed: 26561965]
56. Huang X; Wang X; Zhang J; Xia N; Zhao Q, *Escherichia coli*-Derived Virus-Like Particles in Vaccine Development. NPJ Vaccines 2017, 2, 3. [PubMed: 29263864]
57. Wynn TA, Type 2 Cytokines: Mechanisms and Therapeutic Strategies. Nat Rev Immunol 2015, 15, 271–282. [PubMed: 25882242]
58. Raphael I; Nalawade S; Eagar TN; Forsthuber TG, T Cell Subsets and Their Signature Cytokines in Autoimmune and Inflammatory Diseases. Cytokine 2015, 74, 5–17. [PubMed: 25458968]
59. Xu HM, Th1 Cytokine-Based Immunotherapy for Cancer. Hepatobiliary Pancreat Dis Int 2014, 13, 482–494. [PubMed: 25308358]
60. Brown SD; Fiedler JD; Finn MG, Assembly of Hybrid Bacteriophage Qbeta Virus-Like Particles. Biochemistry 2009, 48, 11155–11157. [PubMed: 19848414]
61. Bennett NR; Zwick DB; Courtney AH; Kiessling LL, Multivalent Antigens for Promoting B and T Cell Activation. ACS Chem Biol 2015, 10, 1817–1824. [PubMed: 25970017]
62. Wu X; McKay C; Pett C; Yu J; Schorlemer M; Ramadan S; Lang S; Behren S; Westerlind U; Finn MG; Huang X, Synthesis and Immunological Evaluation of Disaccharide Bearing Muc-1 Glycopeptide Conjugates with Virus-Like Particles. ACS Chem Biol 2019, 14, 2176–2184. [PubMed: 31498587]
63. Sedlik C; Deriaud E; Leclerc C, Lack of Th1 or Th2 Polarization of CD4+ T Cell Response Induced by Particulate Antigen Targeted to Phagocytic Cells. Int Immunol 1997, 9, 91–103. [PubMed: 9043951]
64. Seder RA; Gazzinelli R; Sher A; Paul WE, Interleukin 12 Acts Directly on CD4+ T Cells to Enhance Priming for Interferon Gamma Production and Diminishes Interleukin 4 Inhibition of Such Priming. Proc Natl Acad Sci U S A 1993, 90, 10188–10192. [PubMed: 7901851]
65. Gajewski TF; Joyce J; Fitch FW, Antiproliferative Effect of IFN-Gamma in Immune Regulation. III. Differential Selection of Th1 and Th2 Murine Helper T Lymphocyte Clones Using Recombinant IL-2 and Recombinant IFN-Gamma. J Immunol 1989, 143, 15–22. [PubMed: 2525146]
66. Snell LM; Osokine I; Yamada DH; De la Fuente JR; Elsaesser HJ; Brooks DG, Overcoming CD4 Th1 Cell Fate Restrictions to Sustain Antiviral CD8 T Cells and Control Persistent Virus Infection. Cell Rep 2016, 16, 3286–3296. [PubMed: 27653690]
67. Zhang L; Qiu W; Crooke S; Li Y; Abid A; Xu B; Finn MG; Lin F, Development of Autologous C5 Vaccine Nanoparticles to Reduce Intravascular Hemolysis In Vivo. ACS Chem Biol 2017, 12, 539–547. [PubMed: 28045484]
68. Hovlid ML; Lau JL; Breitenkamp K; Higginson CJ; Laufer B; Manchester M; Finn MG, Encapsidated Atom-Transfer Radical Polymerization in Qbeta Virus-Like Nanoparticles. ACS Nano 2014, 8, 8003–8014. [PubMed: 25073013]
69. Mangold SL; Prost LR; Kiessling LL, Quinoxalinone Inhibitors of the Lectin DC-SIGN. Chem Sci 2012, 3, 772–777. [PubMed: 22639721]

70. Shalek AK; Satija R; Shuga J; Trombetta JJ; Gennert D; Lu D; Chen P; Gertner RS; Gaublomme JT; Yosef N; Schwartz S; Fowler B; Weaver S; Wang J; Wang X; Ding R; Raychowdhury R; Friedman N; Hacohen N; Park H et al., Single-Cell RNA-Seq Reveals Dynamic Paracrine Control of Cellular Variation. Nature 2014, 510, 363–369. [PubMed: 24919153]

71. Chevrier N; Mertins P; Artyomov MN; Shalek AK; Iannacone M; Ciaccio MF; Gat-Viks I; Tonti E; DeGrace MM; Clauser KR; Garber M; Eisenhaure TM; Yosef N; Robinson J; Sutton A; Andersen MS; Root DE; von Andrian U; Jones RB; Park H et al., Systematic Discovery of TLR Signaling Components Delineates Viral-Sensing Circuits. Cell 2011, 147, 853–867. [PubMed: 22078882]

72. Price AA; Tedesco D; Prasad MR; Workowski KA; Walker CM; Suthar MS; Honegger JR; Grakoui A, Prolonged Activation of Innate Antiviral Gene Signature after Childbirth Is Determined by IFNl3 Genotype. Proc Natl Acad Sci U S A 2016, 113, 10678–10683. [PubMed: 27601663]

73. Ulloa-Montoya F; Louahed J; Dizier B; Gruselle O; Spiessens B; Lehmann FF; Suciu S; Kruit WH; Eggermont AM; Vansteenkiste J; Brichard VG, Predictive Gene Signature in Mage-A3 Antigen-Specific Cancer Immunotherapy. J Clin Oncol 2013, 31, 2388–2395. [PubMed: 23715562]

74. Torres-Aguilar H; Aguilar-Ruiz SR; Gonzalez-Perez G; Munguia R; Bajana S; Meraz-Rios MA; Sanchez-Torres C, Tolerogenic Dendritic Cells Generated with Different Immunosuppressive Cytokines Induce Antigen-Specific Anergy and Regulatory Properties in Memory CD4+ T Cells. J Immunol 2010, 184, 1765–1775. [PubMed: 20083662]

75. Alam MM; Bufano MK; Xu P; Kalsy A; Yu Y; Freeman YW; Sultana T; Rashu MR; Desai I; Eckhoff G; Leung DT; Charles RC; LaRocque RC; Harris JB; Clements JD; Calderwood SB; Qadri F; Vann WF; Kovac P; Ryan ET, Evaluation in Mice of a Conjugate Vaccine for Cholera Made from Vibrio Cholerae O1 (Ogawa) O-Specific Polysaccharide. PLoS Negl Trop Dis 2014, 8, e2683. [PubMed: 24516685]

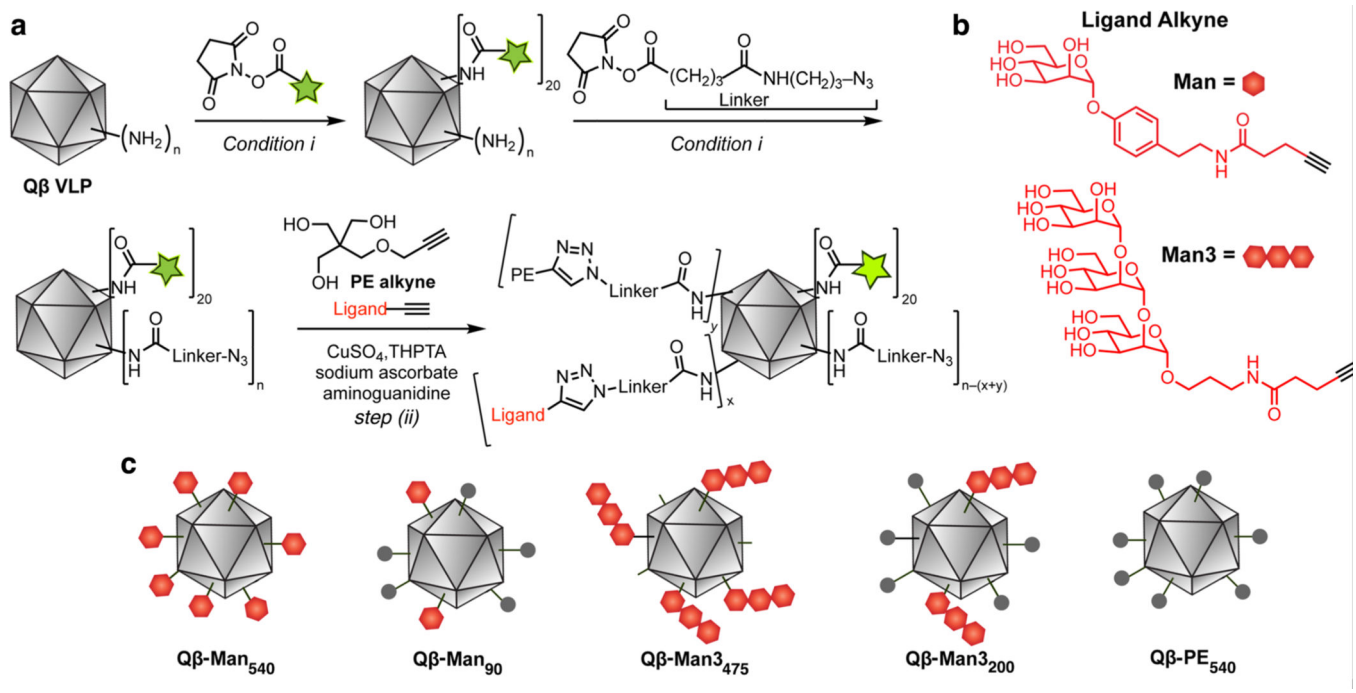

Figure 1. Preparation of fluorescently tagged Qβ particles.

Particles were generated that display an aryl mannoside (Man) group (red hexagon), a trimannoside group (3 linked hexagons), pentaerythritol monoether (PE, grey circle), or a combination. (a) Synthetic scheme (AF488 = Alexa Fluor 488). Conditions: (i) 0.1 M potassium phosphate buffer, pH 7.0, 0 °C to room temperature, 3 h. (step ii) tris-(3 hydroxypropyltriazolylmethyl)amine (THPTA), CuSO4, sodium ascorbate., aminoguanidine, 0.1 M potassium phosphate, pH 7.0, 37 °C, 4 h. (b) Structure of the attached DC-SIGN targeting groups. (c) Graphical representation of the functionalized Qβ VLPs.

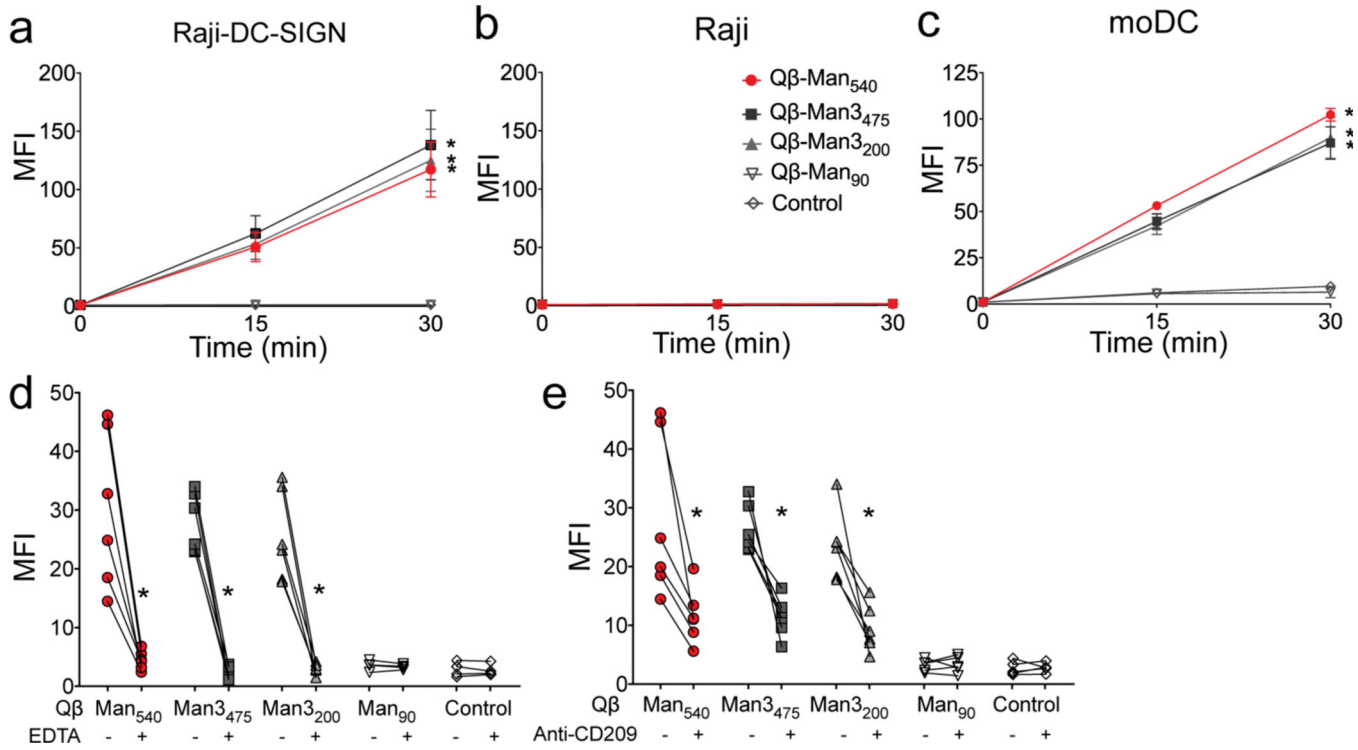

Figure 2. Analysis of VLP interaction with DCs and the role of DC-SIGN.

The internalization of fluorophore-labeled Qβ VLPs functionalized with aryl mannoside, trimannoside, or pentaerythritol (control) was estimated by flow cytometry. Samples tested: (a) Raji-DC-SIGN, (b) Raji cells and, (c) human monocyte-derived dendritic cells (moDC) at indicated time points. Flow cytometry analysis of particle uptake in moDC in the presence or absence of (d) 1 mM EDTA, (e) anti-CD209 (anti-DC-SIGN) antibody 15 min after particle stimulation. The error bars represent standard error of the mean (SEM) from at least two independent experiments. The two-way ANOVA with Dunnett's multiple comparisons test (a-c) and Wilcoxon matched-paired signed rank test (d, e) were used for data analysis. An asterisk denotes a statistically significant difference (*$P<0.05$) between the treatment and the control particle (Qβ-PE540) groups (a-c) and between antibody or EDTA treated and non-treated cells (d, e). Mean fluorescence intensity (MFI; arbitrary units) on the Y-axis was normalized to that of unstimulated cells.

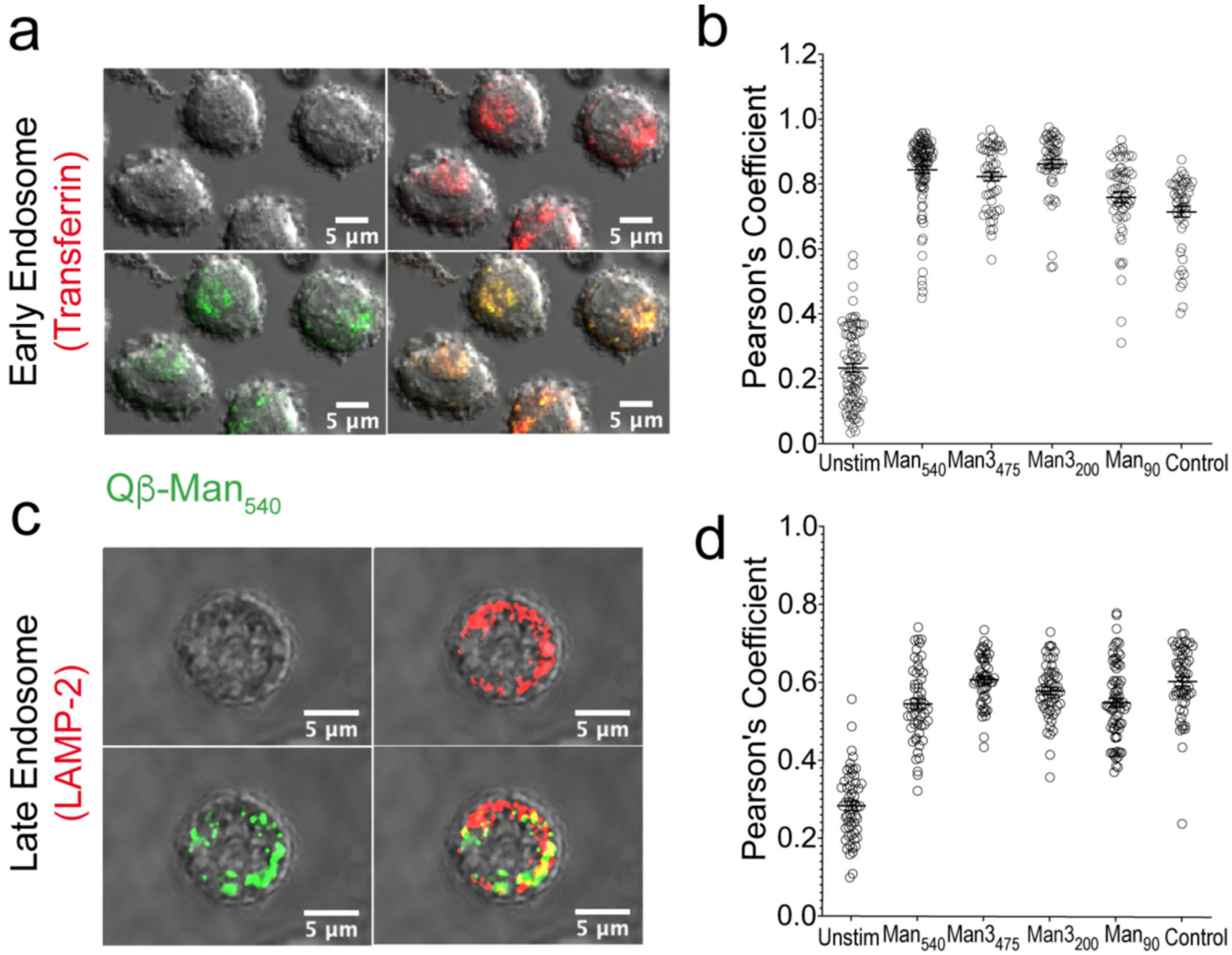

Figure 3. Trafficking of VLPs to early and late endosomal compartments.

(a, c) Representative images of particles (Qβ-Man540 green) trafficked to early and late endosomal compartments in moDC (37 °C, 30 min). The trafficking of particles (green) to transferrin or LAMP2-labeled early or late endosomes (red) was monitored *via* confocal microscopy. (b, d) The colocalization of each particle with transferrin or LAMP2 at the 30 min time point was assessed for >50 cells per treatment using Pearson's coefficient as determined by the Colocalization Threshold plugin in ImageJ.

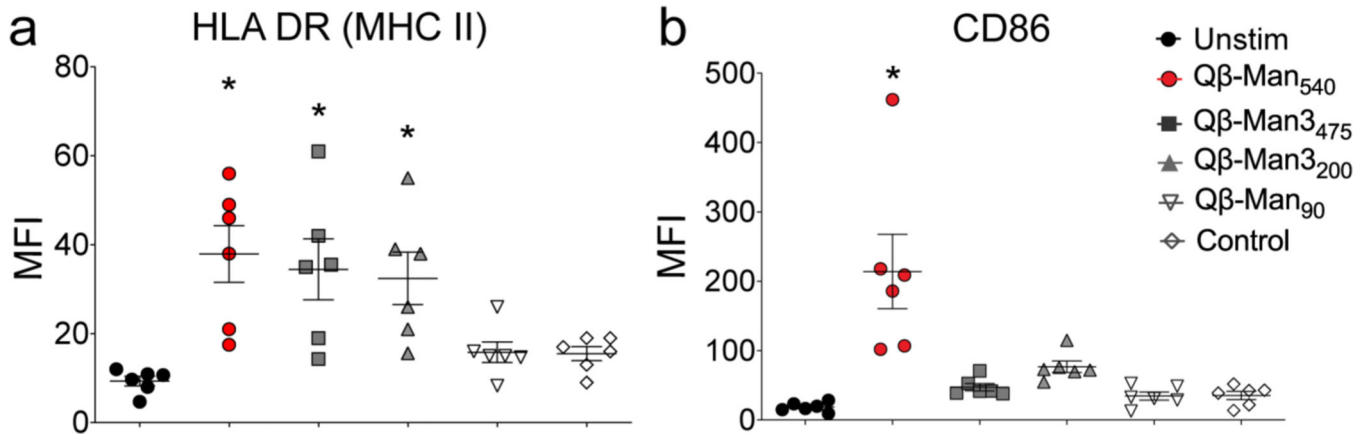

Figure 4. Assessment of human monocyte-derived DC maturation upon VLP exposure.

VLPs (4 nM) were incubated with moDCs (37 °C, 24 h), washed, treated with dye-labeled antibodies against (a) MHC II (HLA DR), and (b) CD86, and then analyzed by flow cytometry. Error bars represent standard error of the mean (SEM) from at least three independent experiments; statistical significance between particle-stimulated and unstimulated cells (*P<0.05) was determined by one-way ANOVA with Dunnett's multiple comparisons test. MFI = mean fluorescence intensity (arbitrary units).

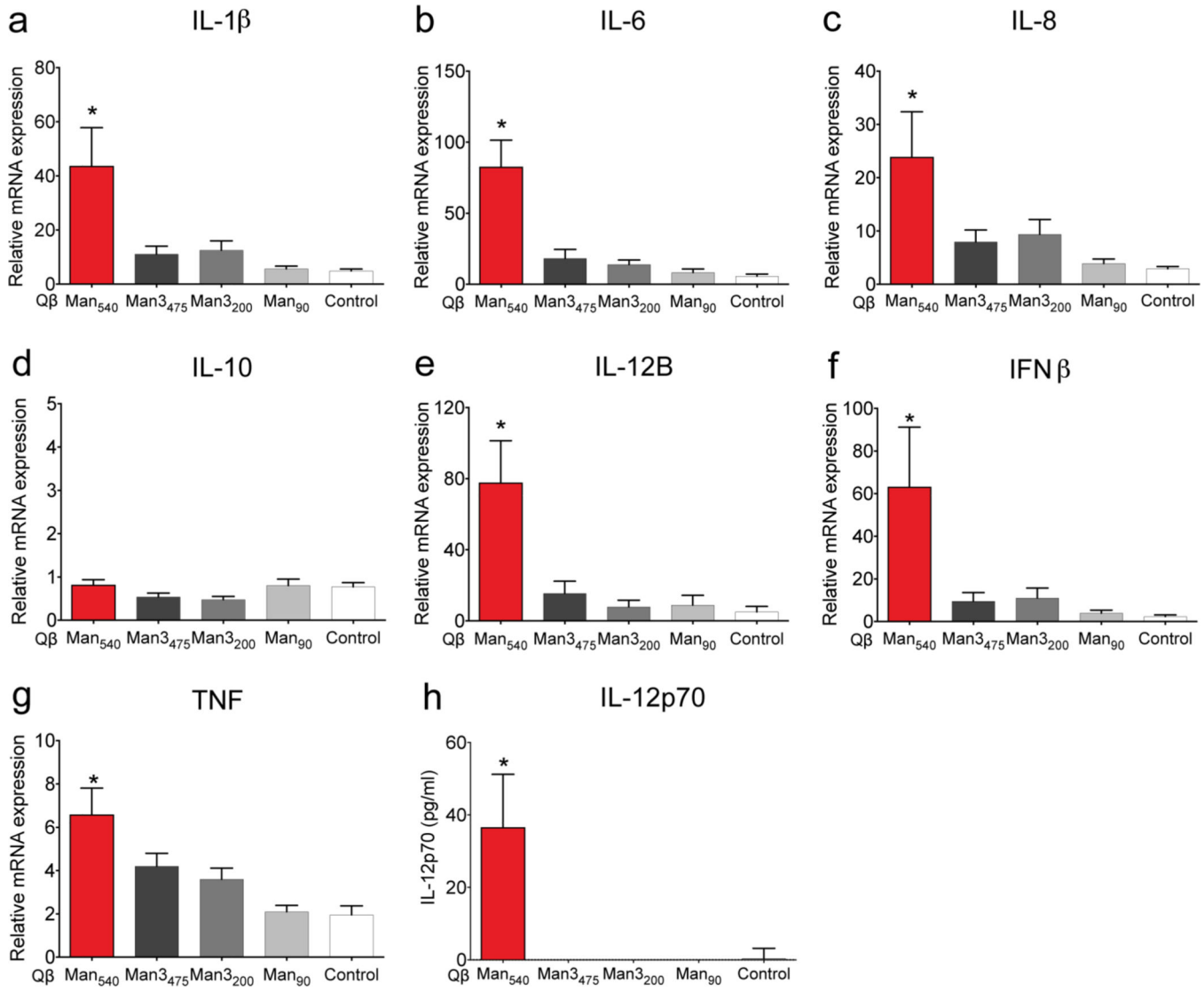

Figure 5. VLP-induced expression of proinflammatory and TH1-type cytokines in moDCs

(a-g) Quantitative real-time PCR analysis of cytokine mRNA expression in moDCs treated with particles (4 nM) for 6 h. (h) IL-12p70 expression in the supernatant of VLP-treated moDCs (4 nM, 48 h) measured by ELISA. The error bars represent standard error of the mean from at least three independent experiments. One-way ANOVA with Dunnett's multiple comparisons test was used for data analysis. An asterisk denotes a statistically significant difference (*P<0.05) between the treatment groups and the control particles (Qβ-PE540).

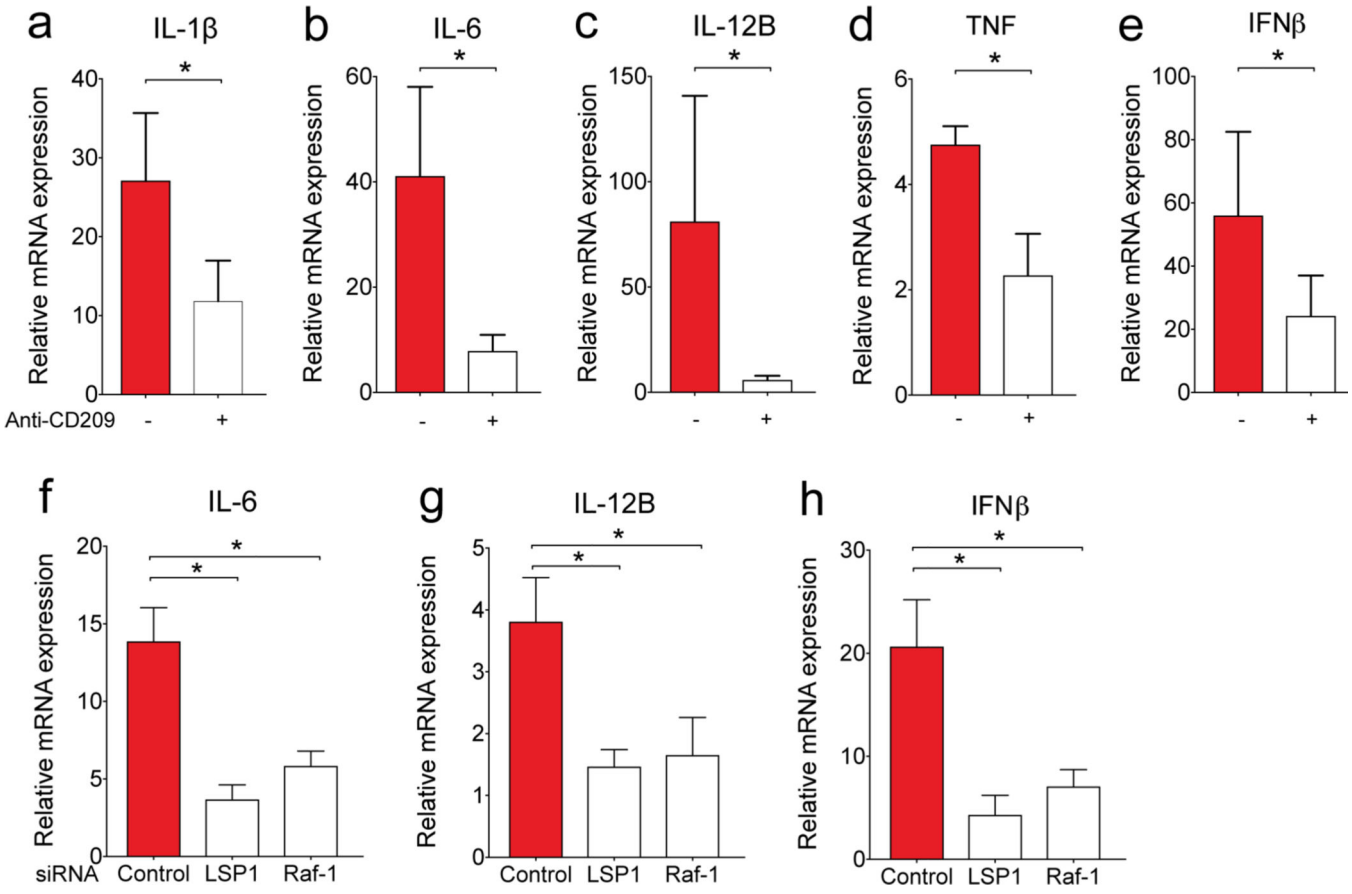

Figure 6. Effect of DC-SIGN on cytokine expression induced by Qβ-Man540.

Quantitative real-time PCR analysis of the expression of cytokine mRNA in moDCs (a-e) pre-treated with or without anti-CD209 (anti-DC-SIGN) antibody or (f-h) pre-treated with control, LSP1 or Raf-1 specific small interfering RNA (siRNA) followed by Qβ-Man540 stimulation. The error bars represent standard error of the mean (SEM) from at least three independent experiments. Wilcoxon matched-paired signed-rank test (a-e) or One-way ANOVA with Dunnett's multiple comparisons test (f-h) was used for data analysis. *P<0.05.

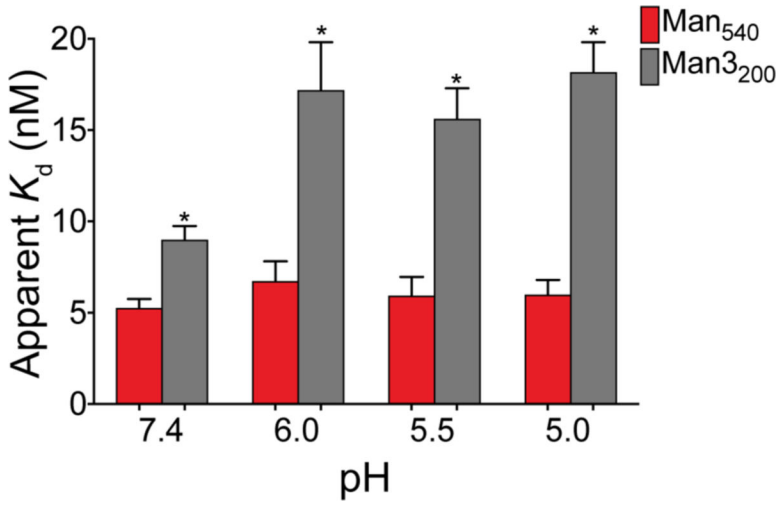

Figure 7. Binding of Qβ-Man540 and Qβ-Man3200 to DC-SIGN at different pH values.

Binding of DC-SIGN ECD to Qβ-Man540 and Qβ-Man3200 was measured by ELISA at pH 7.4–5.0. Apparent dissociation constant (K_d) values were calculated by nonlinear regression curve fit for total binding. The error bars represent standard error of the mean (SEM) from at least three independent experiments.

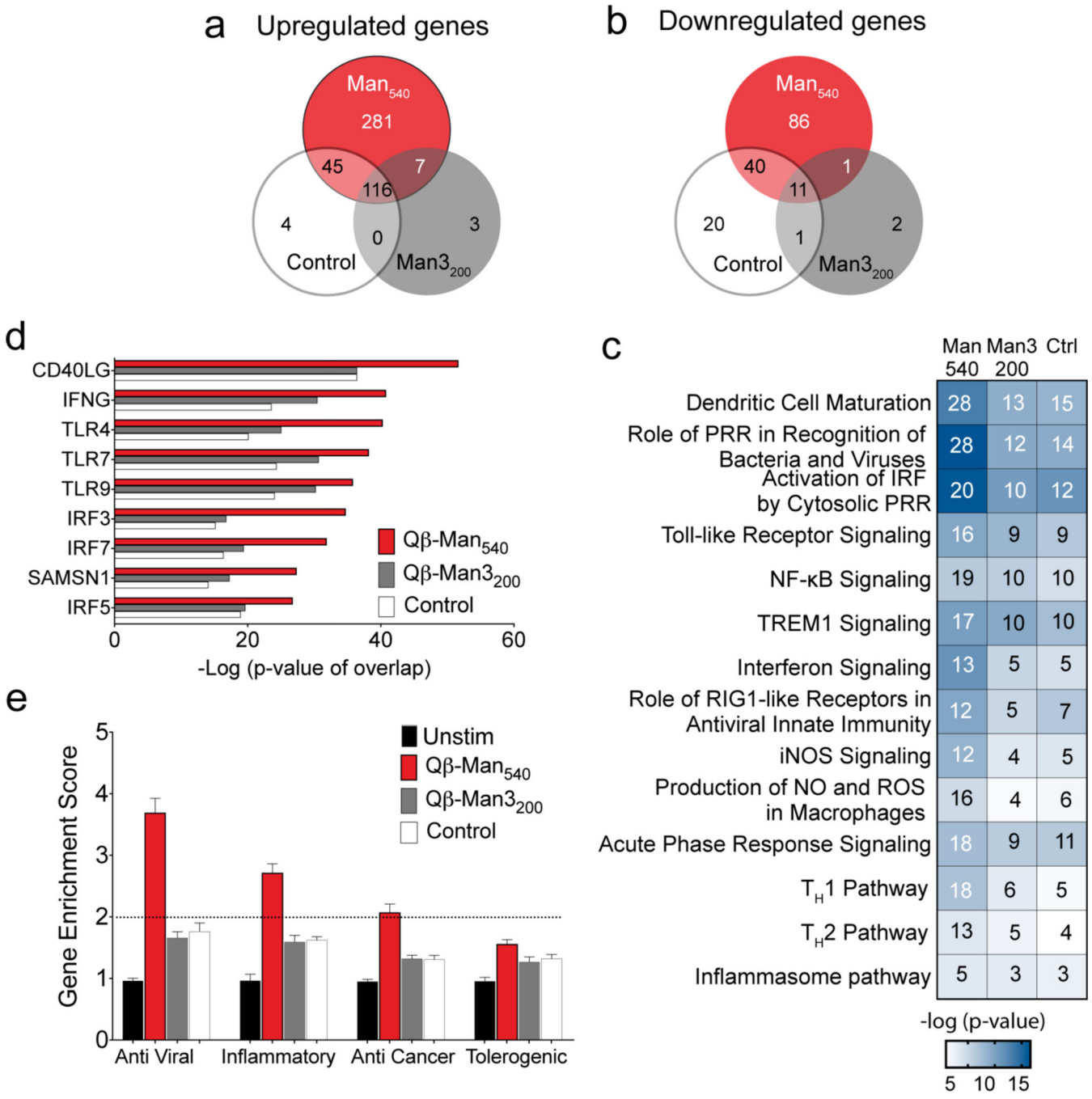

Figure 8. Transcriptional analysis of human monocyte-derived DCs treated with mannosylated particles.

The moDCs were treated with particles (4 nM) for 6 h before RNA sequencing (n=4). Qβ-PE540 was used as a control (Ctrl). (a-b) Venn diagram showing genes upregulated or downregulated at least two-fold compared to untreated cells. (c) Heat map of canonical pathways significantly upregulated (Fisher's exact test, −log10 P values for each represented pathway is shown) in particle treated cells relative to untreated, as predicted by Ingenuity Pathway Analysis (IPA). In each pathway, the number of genes differentially regulated at least two-fold is indicated inside each box. (d) Significant putative upstream regulators with

predicted activating influence on transcriptional signatures in moDCs treated with particles, as determined by IPA. (e) Gene enrichment score for 94 anti-viral, 41 inflammatory, 54 anti-cancer, and 30 tolerogenic genes. Abbreviations: PRR ≡ pattern recognition receptor, NF-κB ≡ nuclear factor kappa-light-chain-enhancer of activated B cells, TREM-1 ≡ triggering receptor expressed on myeloid cells-1, iNOS ≡ inducible nitric oxide synthase, NO ≡ nitric oxide, ROS ≡ reactive oxygen species.

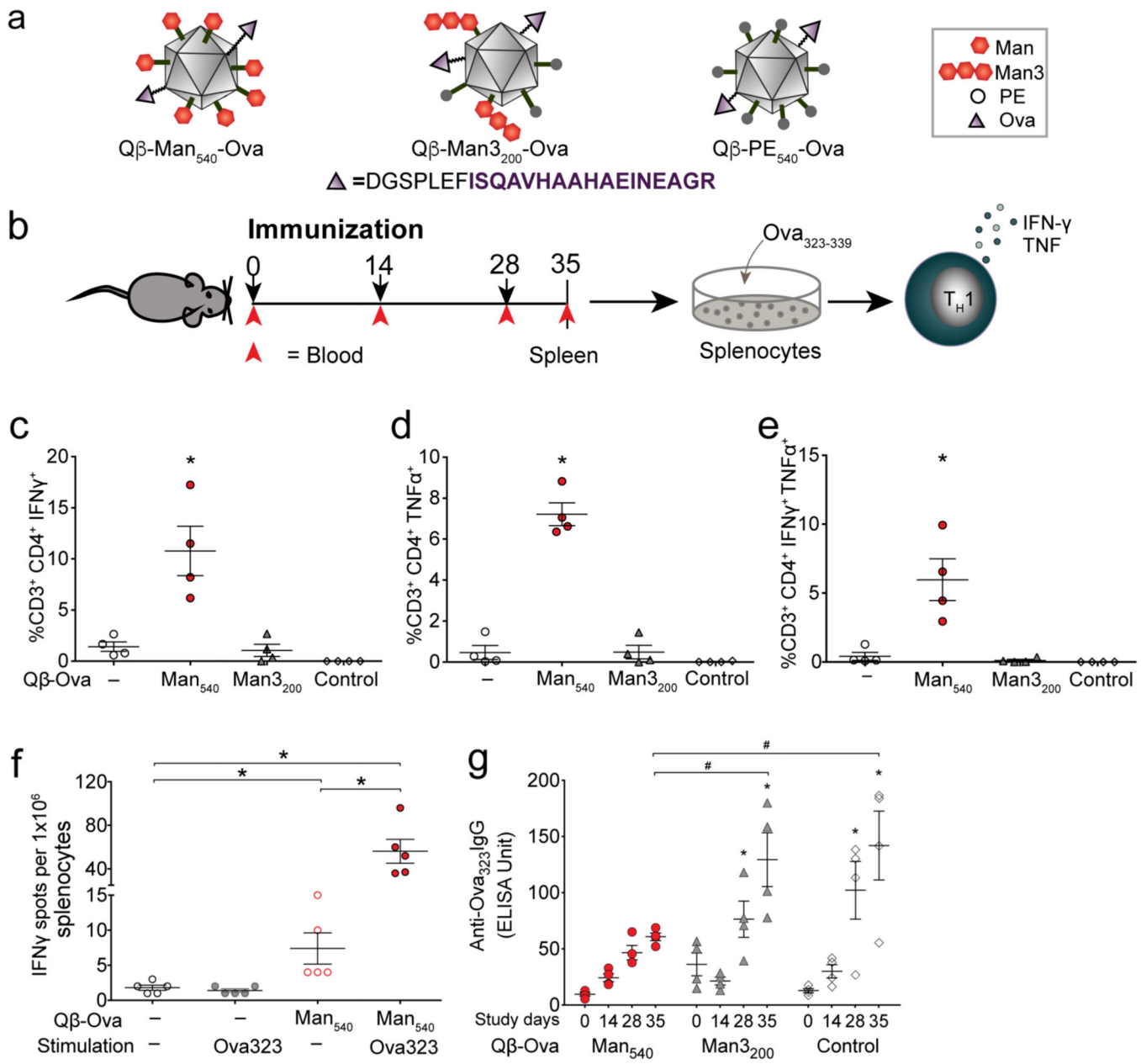

Figure 9. Induction of Th1 type immune responses *in vivo*.

(a) Qβ VLPs used in the *in vivo* study. (b) Experimental design: 4 mice per group; 50 μg of Ova323 peptide-functionalized particles per dose; splenocytes and serum analyzed at day 35. (c-e) Intracellular cytokine staining of splenocytes from immunized mice stimulated with Ova323 peptide for 6 h, analyzed by flow cytometry. (f) IFN_{γ} producing splenocytes quantified by ELISPOT. (g) Anti-Ova323-IgG antibody responses in the serum of immunized mice measured by ELISA. Error bars represent standard error of the mean. The one-way ANOVA with Dunnett's or Tukey's multiple comparisons test was used for data analysis. * indicates statistically significant difference ($P<0.05$) between vaccinated and

unvaccinated cohorts (c-e) or from baseline (day 0) (g). # indicates a statistically significant difference ($P<0.05$) between the compared cohorts.